Nonlinear Saturation and Lasing Characteristics of Green Fluorescent Protein

David J. Pikas,[†] Sean M. Kirkpatrick,* Erin Tewksbury,[‡] Lawrence L. Brott,[§] Rajesh R. Naik,[§] and Morley O. Stone

Materials and Manufacturing Directorate, Air Force Research Laboratory, WPAFB, Ohio 45433-7702

William M. Dennis

Department of Physics and Astronomy, University of Georgia, Athens, Georgia 30602

Received: December 31, 2001; In Final Form: March 4, 2002

Green fluorescent protein (GFP) has been of interest to researchers recently due to its use in nonlinear microscopy and biomedical applications. Through the use of nonlinear characterization, GFP has been previously shown to exhibit saturable nonlinear absorption. This nonlinear saturation suggests the possibility of a two-photon induced population inversion in GFP, which can lead to the use of GFP as a frequency upconversion laser material, particularly for bioMEMS devices. Here, we explore this population inversion and report on the ultrafast two-photon pumped lasing properties of GFP. Specifically, we report on the lasing threshold, spectral features and output−input energy characteristics. This is the first demonstration of ultrafast two-photon pumped lasing in a biological chromophore. Furthermore, GFP also appears to have a nearly cubic dependence of the saturation intensity on the concentration of GFP molecules. In this report, we also investigate this relationship by looking at the theoretical components affecting the saturation intensity to determine their dependence on GFP concentration.

I. Introduction

Green fluorescent protein (GFP) is a naturally occurring chromophore found in the jellyfish *Aequorea victoria* and has been used in monitoring gene expression and intracellular protein localization.[1] The chromophore of GFP is formed by the autocatalytic, posttranslational cyclization and oxidation of the tripeptide Ser^{65}-Tyr^{66}-Gly^{67} in the primary structure of the expressed protein.[2] In solution, the chromophore exhibits two absorption maxima at 396 and 476 nm that relax to a common emission state to produce greenish-yellow light centered at 509 nm.[3]

GFP has been shown to be an efficient two-photon absorber, readily excited by ultrafast 790 nm laser pulses, which has a two-photon fluorescence spectrum similar to that of the one-photon case.[4,5] Molecules that exhibit a strong two-photon absorption have potential use in applications, such as three-dimensional fluorescence imaging, optical data storage, and microfabrication.[6,7] It has also been found that the two-photon absorption (TPA) coefficient of GFP exhibits nonlinear saturation as a function of intensity.[8] This is consistent with reports of the saturation of the nonlinear fluorescence.[5,9] Until recently, this saturation was believed to be attributed to an excited-state absorption within the chromophore; however, it has been shown that at low repetition rates (<500 Hz) and short pulse width (<100 fs), the nonlinearity is due to a saturable two-photon absorption of the GFP chromophore, and that the excited-state absorption is primarily due to either background protein groups surrounding the chromophore or additional constituents associated with the chromophore such as dimers. As a consequence, the system also appears to be inhomogeneously broadened[8] within the time frame of the experiment (100 fs).

The two-photon saturated absorption model presented in the previous paper suggests that a nonlinear population inversion may be achieved in the material. This population inversion allows for the potential use of GFP as a two-photon pumped, frequency upconversion lasing material. A frequency upconversion material is one that emits a higher energy photon when pumped with lower energy photons. There are two major mechanisms that primarily responsible for this phenomenon. One is based on sequential stepwise multiphoton excitation in materials such as rare-earth doped crystals, inorganic glasses and optical fibers.[10−18] The second process is initiated by a direct simultaneous two-photon absorption and subsequent population inversion and has been observed in semiconductor and rare earth crystals,[19−22] dye solutions, and dye-doped solid matrixes.[23−29] In this work, the two-photon induced population inversion of GFP is further investigated and the characteristics of the ultrafast two-photon pumped lasing of GFP are presented. Parameters such as the spectral output, laser threshold and output-input energy characteristics are given and compared to theoretical results. To the best of our knowledge, this is the first report of two-photon pumped lasing demonstrated in a biological system.

In addition to the TPA lasing, this work and others collectively demonstrate the dependence of the saturation intensity on the concentration of GFP molecules. Volkmer lists the saturation intensity as 400 GW/cm^2 for an 18 μM sample of GFP,[5] Schwille lists a saturation intensity of 0.01 GW/cm^2 for few hundred nanomolar concentration,[9] and we recently reported a 10 GW/cm^2 saturation intensity for a 5 micromolar concentration.[8] A plot of the saturation intensity versus the concentration of GFP molecules (Figure 4) suggests that there is nearly a cubic

* To whom correspondence should be addressed. Bldg. 651, Suite 13005 P St., WPAFB, OH 45433-7702. Email: sean.kirkpatrick@afrl.af.mil. Phone: (937) 255-3808 x3164. Fax: (937) 255-1128.
[†] University of Dayton.
[‡] Wright State University.
[§] Technical Management Concepts Inc.

10.1021/jp014643s CCC: $22.00
Published on Web 04/09/2002

(2.7 ± 0.1) dependence of the saturation intensity on the concentration (and hence number density) of GFP molecules. To explore this apparent dependence, the theoretical components that effect the saturation intensity (inhomogeneous line shape, homogeneous line width, TPA cross section, and lifetime of the two-photon state) are investigated and discussed to determine their variability as a function of GFP concentration.

II. Theory

A. Characterization Summary. Through the use of ultrafast z-scan and nonlinear fluorescence analysis, it has been shown that GFP is apparently inhomogeneously broadened and exhibits a nonlinear saturation of the two-photon absorption event. Details of these results were published previously, so only a summary review is given here.[8] The total effective two-photon absorption coefficient of the system was found to be an intensity dependent quantity having the functional form of

$$\beta_{\text{eff}}^{\text{Inh}}(I) = \frac{\beta_0^{\text{Inh}}}{\sqrt{1 + I_0^{\,2}/I_{\text{sat,Inh}}^{\,2}}} + \beta_0^{\text{Inh,Bkg}}\left(1 + \frac{\sigma_{\text{ESA}}\tau_p I_0}{2\hbar\omega}\sqrt{\frac{\pi}{2}}\right) \quad (1)$$

Here, the relationship $\beta_0 = \sigma_{\text{TPA}}(g_1/g_0)N_0$ has been used where g_1 (g_0) is the electronic degeneracy of the upper (lower) state. The two-photon absorption (TPA) cross section (σ_{TPA}) is given in units of cm^4/GW and embodies the dipole moments, line shape, and constant factors. Note also that the above saturation TPA coefficient has been designated with a (Bkg) in the superscript for distinction. The excited-state absorption cross section is σ_{ESA}, and is assumed to be dispersionless over the bandwidth of the excitation. N_0 is the number density of GFP molecules (molecules/cm^3), τ_p is the pulse width, I_0 is the peak incident intensity, and $I_{\text{sat,Inh}}$ is the inhomogeneous saturation intensity (both in GW/cm^2). The square of the saturation intensity is given as

$$I_{\text{sat,Inh}}^{\,2} = \frac{2\hbar\omega\Delta\omega\rho(2\omega)}{\tau_{10}\sigma_{\text{TPA}}\left(1 + \frac{g_1}{g_0}\right)} \quad (2)$$

Here, $\rho(2\omega)$ is the probability of a homogeneous class of absorbers having a central frequency of 2ω (related to the inhomogeneous line shape), $\Delta\omega$ is the homogeneous line width and is related to the dephasing time of the excitation, and the total lifetime of the two-photon state is τ_{10}.

B. GFP Lasing Model. The above saturation model of GFP suggests that a two-photon induced population inversion can be achieved, as shown in Figure 1. Here, the *homogeneous* set of rate equations presented in ref 8, and leading to eq 1, have been solved numerically to give the population inversion as a function of pump energy. Inversion is found to occur around 0.2 μJ, and results in a few percent inversion over the time frame corresponding to the excitation pulse width. This population inversion coupled with the large value obtained for the intrinsic TPA cross section indicated the potential use of GFP as a frequency upconversion lasing medium. From the functional form of the effective TPA coefficient (eq 1), the effective two-photon absorption cross section acting as a gain mechanism (in units of cm^2) for emission at 509 nm is given by

$$\sigma_{\text{gain}}(I) = \frac{\sigma_{\text{TPA}}\frac{g_1}{g_0}I_0}{\sqrt{1 + I_0^{\,2}/I_{\text{sat,Inh}}^{\,2}}} \quad (3)$$

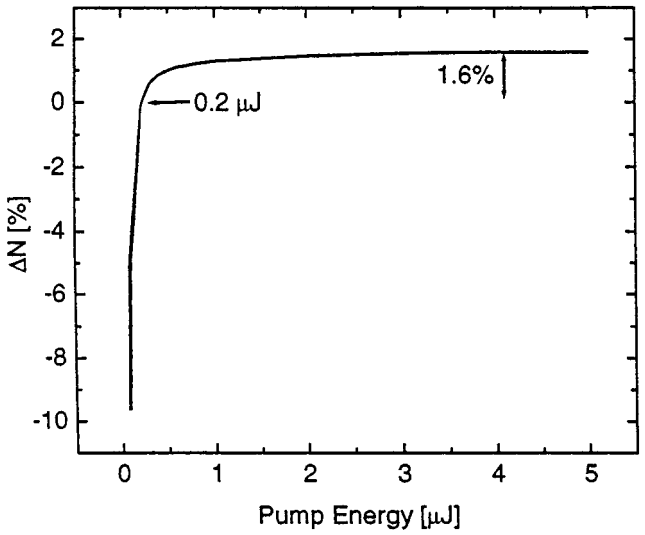

Figure 1. Two-photon induced population inversion (in percentage) of GFP as a function of laser pump energy calculated using the homogeneous rate equation analysis in reference 8. Predicted threshold is 0.2 μJ and the total attainable inversion is about 1.6%.

The contribution of the background protein(s) is not included in the above cross section because it acts to remove electron population from the two-photon state by either quenching a TPA event or by providing an excited-state absorption path; therefore, acting as a loss mechanism. With the above model of the TPA cross section, the intensity dependent gain coefficient of GFP for a given population inversion between the ground state and the two-photon excited state can be represented by

$$\gamma(I) = \sigma_{\text{gain}}(I)\Delta N_{10} \quad (4)$$

where ΔN_{10} is defined as the difference in population densities between the two-photon state N_1 and the ground state N_0.

As described above, the excited-state absorption, which is assumed to be dispersionless across the excitation, will act to remove population therefore contributing to the loss of the system at 509 nm. Other factors such as linear absorption, scattering, and coupling losses will act as mechanisms to reduce the total lasing output. The lasing output[30] energy as a function of the absorbed pump energy E_{pump} can therefore be represented as

$$E_{\text{out}} = \eta_{\text{ext}}E_{\text{pump}}(1 - R_{790\text{nm}})(1 - R_{509\text{nm}}) \times (e^{-\alpha L}e^{\gamma(I)L}e^{-\sigma_{\text{ESA}}\Delta N_{21}L}e^{-\sigma_{\text{scatt}}N_0 L}) \quad (5)$$

where L is the path length of active lasing medium, α is the linear absorption coefficient at 509 nm (no linear absorption at 790 nm), ΔN_{21} is the population difference between a higher excited state and the two-photon state, R_λ is the reflectivity of the laser cavity mirrors at λ, and σ_{scatt} is the scattering cross section. The collection efficiency and the quantum efficiency of the detection system is given as η_{ext}, which includes the collection efficiency of the fiber optics, the transmission efficiency of the fiber at 509 nm, and the quantum efficiency of the CCD detection system. Note that we have changed to energy here in order to compare to energy measurements.

Due to the high intensities of the ultrafast pump pulse, nonlinear effects must be taken into account as the pump pulse propagates through the quartz substrates used as the GFP cavity mirrors. The pump pulse will experience temporal broadening due to group velocity dispersion (GVD) along spectral broadening from self-phase modulation (SPM) as it travels through the

quartz mirror. The maximum amount of spectral broadening due to self-phase modulation can be approximated by[31]

$$\Delta\omega_{\max} = \frac{\omega_0 n_2 a_0^{\,2} z}{c\tau_p}(\sqrt{2}e^{-1/2}) \tag{6}$$

here ω_0 is the fundamental frequency of the pump pulse, n_2 is the nonlinear refractive index, a_0 is the initial field amplitude, and z is the propagation distance. This quantity gives the bandwidth of the total energy incident on the GFP lasing medium. Assuming that the only significant absorption is two-photon across the supercontinuum spectrum, then the total amount of two-photon excitation is found by mapping the resulting supercontinuum into two-photon space. If one makes the further assumption, based on similarities found in other nonlinear chromophores, that the one-photon absorption spectrum is similar to the two-photon absorption spectrum, then the fraction of energy absorbed by the GFP is found by the energy overlap integrals of the normalized line shape functions (energy conservation), and is found to be

$$E_{\text{pump}} = \frac{\Delta\omega_{\text{abs}}}{2\Delta\omega_{\max}} E_{\text{in}} \tag{7}$$

where E_{in} is the amount of energy in the pump pulse prior to entering the cavity, and $\Delta\omega_{\text{abs}}$ is the bandwidth of the monomer GFP absorption spectrum.

The temporal distribution of the frequency in the pulse shape (chirp) is also an important characteristic of a SPM broadened pulse. The linear chirp coefficient C is given as[31]

$$C = \frac{\omega_0 n_2 a_0^{\,2} z}{2c\tau_p^{\,2}} \tag{8}$$

The chirp coefficient can be used to approximate the change in the pump pulse width due to SPM. The resulting effective pulse width of the energy absorbed by the lasing medium has the form of[32]

$$\tau_{\text{eff}} = \frac{\sqrt{2}\ln 2}{\pi\Delta\omega_{\max}}\sqrt{1 + C^2} \tag{9}$$

C. Concentration Dependent Saturation Intensity. As mentioned above, previous work has indicated that the saturation intensity of GFP has a concentration dependence that is nearly cubic. The theoretical form of the inhomogeneous saturation intensity is given by eq 2 above. Within that expression, the only concentration dependence arises out of contributions from the inhomogeneous line shape, homogeneous line width, TPA cross section, and lifetime of the two-photon state. Each contribution is discussed below.

Beginning with the homogeneous line width $\Delta\omega$, the expression $\Delta\omega = 2\pi/T_2$ relates the dephasing time T_2 to $\Delta\omega$. If one assumes that the major contribution to the dephasing time in this system arises from collisions, then in the simplest form, kinetic theory[33] gives the dephasing time as

$$T_2 = \frac{\sqrt{\pi/8}}{N_0\sigma_{\text{scatt}}\bar{v}} \tag{10}$$

Here, N_0 is the number density of molecules, σ_{scatt} is the scattering cross section, and $\bar{v}$ is the average velocity of the molecules. Subsequently, this suggests that $\Delta\omega$ is proportional to the number density N_0.

The concentration dependence of the inhomogeneous line shape is investigated by measuring the excitation spectra of GFP as a function of concentration. In a linear, well-behaved system, the excitation spectrum will increase linearly with the concentration of absorbers. The probability of a class of absorbers having some central frequency ω is then proportional to the excitation signal normalized to the concentration. In other words, for such a linear system, the probability of a class of absorbers having a center frequency of ω is independent of the total number of absorbers, as long as the distribution remains constant. However, GFP has been shown to dimerize with increasing concentration, thus altering the linear relationship of excitation to concentration.[34] It is expected, therefore, that as the concentration is increased more dimers will form, affecting the probability function $\rho(2\omega)$. Measuring the excitation spectrum as a function of intensity and normalizing to the total concentration will thus give the functional dependence of the probability function on concentration.

In addition, this excitation measurement also gives the ratio of monomers to dimers in solution at each concentration measured. Excitation spectra of GFP in solution exhibit two peaks at 395 and 476 nm. The ratio of these peaks have been shown to change as dimerization occurs, the peak at 395 nm being largest for a solution dominated by monomers and the peak at 476 nm being largest when the solution is dominated by dimers.[3,34] The dimerization of GFP has been reported as being responsible for the fluorescence quenching observed previously.[35] There are two main consequences of this: (1) dimerization results in multipolar energy transfer, reducing the total lifetime of the fluorescence, or (2) a new molecular moiety forms, affecting the orbital configuration and hence the radiative/nonradiative coupling. If, as has been reported by De Angelis et al.,[35] electrodynamic multipolar interactions are not the primary mechanism for quenching, but rather the structural deformation resulting from dimerization, then one would expect that the formation of dimers may also lead to a concentration dependent TPA cross section. This second molecular moiety will then affect the bulk measurement of the two-photon absorption coefficient as described previously and in eq 1.

Alternatively, if dimerization does not affect the transition moments within the individual GFP constituents, then the TPA cross section should not have a concentration dependence, but the lifetime of the two-photon state will according to electrodynamics. Energy transfer resulting from the dimerization will affect the decay rate of the chromophore depending on the type of interaction. Assuming a multipolar interaction, the concentration dependence of the decay rate for a dipole−dipole interaction or quadrupole-quadrupole interaction is given by[36]

$$R_{\text{dipole},dipole} = \frac{1}{\tau_{10}} = \frac{\alpha_{\text{DA}}^{(6)}}{r^6} \propto N_0^{\,2}$$

$$R_{\text{quadrapole,quadrapole}} = \frac{1}{\tau_{10}} = \frac{\alpha_{\text{DA}}^{(10)}}{r^{10}} \propto N_0^{10/3} \tag{11}$$

In this expression, r is the intermolecular separation, and N_0 is the number density of molecules. The factor α_{DA} is a grouping of fundamental constants, the oscillator strength of the radiative transition, and energy overlap integrals that are independent of concentration but specific to the type of interaction. These parameters are derived and explained in detail in ref 37. In such a system, a measurement of the lifetime at 509 nm versus concentration should verify the appropriate interaction.

As a final note, it has also been reported that protonation of GFP via photoisomerization (at 398 nm) or titration has a similar

effect on the excitation spectra as dimerization.[3] Subsequently, one may argue that the second constituent responsible for some of the nonlinear behavior discussed above may be due to this species instead of the dimer. However, all experiments carried out here are under neutral pH, varying only the concentration, and photoisomerization is observed over a period of several hours, much longer than the time frame of this experiment. It is therefore reasonable to exclude consideration of protonated monomeric GFP in this work, considering dimer formation as the primary constituent.

III. Experimental Section

A. Synthesis of GFP. A polyhistidine-tagged GFP was expressed in *E.coli* using the expression plasmid pET22b (Novagen) wherein the coding region of GFPuv (cycle 3 mutant) was fused in-frame with a carboxyl-terminal polyhistidine tag. The recombinant GFP was expressed in bacterial strain BL21 (DE3) after induction with IPTG (1mM) at 30 °C and purified by nickel affinity chromatography. Protein purity was confirmed by SDS-PAGE. The purified sample was dialyzed against 10 mM sodium phosphate buffer pH 7.0 and stored at −20 °C.

The GFP solution was dialyzed in water at 4 °C overnight and concentrated under vacuum. This protein solution (31.5 μL) was mixed with a poly(ethylene glycol) (600) diacrylate (3.5 μL, product SR-610 from Sartomer) and 2,2-diethoxyacetophenone (0.1 μL, Aldrich) to produce a final GFP concentration of 352 μM.

B. Cavity Configuration. The laser cavity containing the above formulation of GFP consisted of two stacked dielectric mirrors separated by a 50 micron Teflon spacer which was cured by exposure to a 4W 365 nm UV light source for 4 min. The plane mirrors were optimized for maximum reflection (>99% at 0°) in the green (532 nm). Reflectance was measured to be 92.8% and 12.7% at 509 and 790 nm, respectively. With the optical parameters of the mirrors and lasing medium known, the ABCD optical matrix of the cavity was determined for completeness. It was verified that the cavity produced a moderately stable resonator for an end-pump configuration, as expected for a plane-parallel cavity. It should be noted that the pulse width within the cavity, calculated from eqs 6−9 is approximately 200−300 fs over the bandwidth of the excitation. Subsequently, the path length of 50 microns is well within the coherence length of the pump pulse.

C. Spectral Measurements. The cavity was end pumped with a Ti:Sapphire femtosecond laser system with chirp pulse amplification. This system generated bandwidth-limited 80 fs pulses, centered at 790 nm at a repetion rate of 492 Hz. The beam was focused to a waist size of 42 μm ± 3 μm at the cavity. Two phased shutters allowed for single pulse events to be incident on the GFP medium. A 550 nm short pass filter was placed after the cavity to block the near-IR pump beam and allow the propagation of the generated visible light. The visible output was collected and coupled into an optical fiber that transported the light into an ISA Spex 270M spectrometer where the emission was collected on a Princeton Instruments liquid nitrogen CCD array.

D. Polarization Measurements. A variable polarizer was inserted between the laser cavity and coupling optics in the setup described above in order to determine the polarization dependence of the output light. The incident energy was held constant at 120 μJ, which corresponds to an absorbed pump energy of 7.9 μJ from eq 7, and again was restricted to single pulse events. A 360° rotation of the polarizer was performed with emission collected at intervals of every 10°.

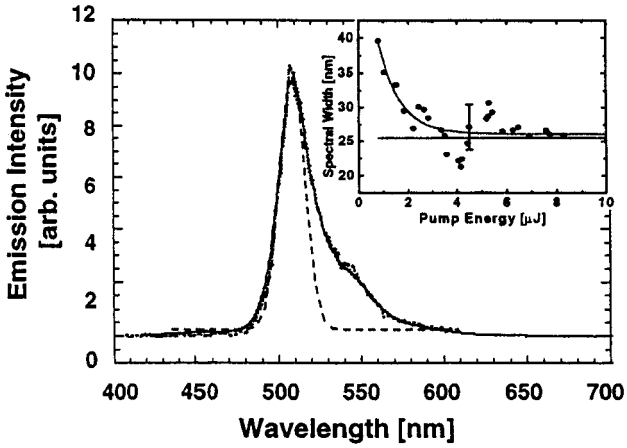

Figure 2. Linear fluorescence (solid line), nonlinear fluorescence (dotted line), and two-photon pumped lasing (dashed line) of GFP resulting from excitation at 396, 790, and 790 nm respectively. The inset shows the spectral width of the lasing output as a function of increasing pump energy. The flat solid line shows the bandwidth limit of the pump pulse, while the curved line is a guide to the eye.

E. Excitation Spectra Measurements. The excitation spectra of GFP were measured using a Perkin-Elmer LS50B spectrofluorometer from a solution of GFP in a 1 cm quartz cuvette. The emission wavelength at 509 nm was monitored using a slit width between 5 and 12 nm, while scanning the excitation wavelength from 300 to 500 nm. Concentrations analyzed ranged from 35 μM to 0.16 μM. The excitation peaks at 396 and 476 nm were measured in order to determine the ratio of dimer (476 nm) to monomer (395 nm) concentrations. It should be noted that there are contributions from both species at each absorption peak but monomer absorption is dominant at 395 nm and dimer absorption is dominant at 476 nm.

F. *z*-Scan Measurements. To determine the concentration dependence of the two-photon absorption. cross section *z*-scan measurements were performed on a series of GFP concentrations. A standard ultrafast *z*-scan technique was performed, details of which are explained elsewhere in the literature.[37] Samples were prepared in 5 mm spectroscopic cells with concentrations ranging from 64 to 0.03 μM. The same laser system described above was used to perform the measurements keeping the scan energy constant at 4.90 μJ for all samples.

IV. Results and Discussion

A. GFP Lasing Results. Ultrafast irradiation of the GFP filled cavity resulted in visible light emission having multiple components. These components include contributions from the GFP lasing as well as supercontinuum generation due to the quartz substrates used as the cavity mirrors. This is expected given the high intensities generated from a focused femtosecond pulse. The spectral peaks associated with these bands are centered at 485 and 532 nm, respectively, and are independent of the peak associated with GFP emission, as measured with a blank control sample.

The linear fluorescence spectrum (solid line) of GFP excited by 396 nm light is seen in Figure 2. The nonlinear fluorescence (dotted line) from excitation at 790 nm is also shown in Figure 2. The peak emission wavelength for both cases is 509 nm with similar spectral bandwidths. There is a strong correlation between the two processes, which indicates that the radiative decay is occurring from the same excited state for both the linear and nonlinear case.

The output lasing spectrum (dashed line of Figure 2) also has a peak emission centered at 509 nm; however, there is a

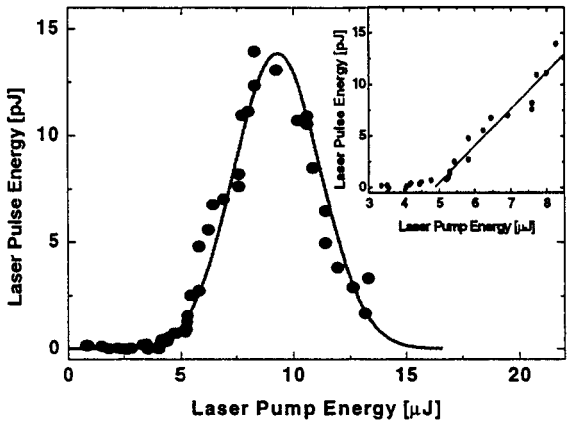

Figure 3. Output energy of GFP lasing cavity as a function of laser pump energy. The experimental data is given as solid dots and the theoretical fit using eq 5 is given as a solid line. The tangent line regressed through the data to obtain the threshold lasing value is shown in the inset.

narrowing of the spectral bandwidth as compared to the fluorescence. To differentiate between lasing and fluorescence this spectral narrowing was investigated further, the results are shown in the inset of Figure 2, where the spectral bandwidth is plotted as a function of the pump energy. This pump energy value is obtained from eq 7. As the pump pulse energy is increased past 4 μJ $\pm$ 1 μJ, a narrowing of the bandwidth is observed. At higher energies, the spectral bandwidth of the GFP lasing begins to approach the value of the bandwidth limit (25.5 nm) of the pump laser. An investigation of the spectral bandwidth of the peaks from the supercontinuum generation shows an increase in the spectral width as the intensity is increased (data not shown) as predicted by self-phase modulation (SPM) theory[31,32] and eq 6.

The output−input lasing characteristics are shown in Figure 3. The experimental data points are represented by the circles and the theoretical fit to these data using eq 5 is given as a solid line. At lower energies ($<$10 μJ), the two-photon pumped lasing is dominant while, at higher pump energies, the removing of electron population due to excited-state absorption becomes the dominant process and reduces the lasing output. The lasing threshold is measured to be 4.9 μJ $\pm$ 0.8 μJ by regressing a tangent line (shown in the inset of Figure 3) through the experimental lasing data back to the laser pump energy axis. This threshold value and overall curve corresponds with the fit of theoretical output generated from our model describing the GFP chromophore. The unknown parameters used in eq 5 are the population difference between the two-photon state and the ground state ΔN_{10}, the population difference between a higher excited state and the two-photon state ΔN_{21}, and the saturation intensity. The inversion density ΔN_{10} at threshold I_t can be estimated from[38]

$$\gamma(I_t) = \alpha - \frac{1}{L}\ln r_1 r_2 \qquad (12)$$

where r_1 and r_2 are the reflectivities of the cavity mirrors at the lasing wavelength. Using eqs 3−4 above, with $I_t \ll I_{sat,Inh}$, the threshold inversion density is found to be approximately 0.3% of the total concentration (352 μM), assuming equal degeneracy between the upper and lower states. During the course of the fit to the data in Figure 3, these population differences were allowed to vary. The values of these parameters obtained in the fit are $\Delta N_{10} = 2.7\%$ of the total population of GFP molecules $\Delta N_{21} = 3\%$ of ΔN_{10} (not in inversion), and $I_{sat,Inh}$ was determined to be 2.5×10^6 GW/cm^2. While it is clear that the population differences ΔN_{10} and ΔN_{21} are intensity dependent quantities, the total variation should not be large compared to the variation in the gain cross section. In fact, the only accurate method of fitting these data would be to solve the inhomogeneous rate equations at every point per intensity level. However, as has been shown previously,[8] since this system is inhomogeneously broadened on this time scale, a rate equation analysis is impractical. In this analysis, the constant values of the population differences should be viewed as mean values. In addition to the parameters above, a typical scattering cross section of approximately 10^{-16} cm^2 was also used. The remaining parameters from eq 5, such as the loss mechanisms, cross sections (found from previous work), and efficiency of the detection system are given in Table 1. Note that the measured threshold value is higher than that obtained from Figure 1. This is consistent with comparing an inhomogeneous measurement to a homogeneous solution, and is expected.

TABLE 1: Fit Parameters of the output Energy for the GFP Lasing Model (Equation 5)

parameter	value
σ_{TPA}	2.4×10^{-17} cm^4/GW
σ_{ESA}	1.25×10^{-16} cm^2
η_{ccd}	0.40
η_{fiber}	0.45
$\eta_{coupling}$	0.50

At higher intensities the laser cavity may also be experiencing damage from the pump pulse. The damage threshold of the cavity mirrors is listed as 5 J/cm^2;[39] therefore, with a beam waist of about 42 microns, damage occurs at incident energies over 280 μJ. The lasing medium is about 90% water, and therefore may experience some self-healing due to its liquid nature. However, to mitigate any problems associated with the damage threshold, all data was obtained using a single shot approach, and incident energies were restricted to a maximum value of 200 μJ (pump energy of 13.2 μJ).

To aid in distinguishing between fluorescence and lasing output, the polarization of the emission at 509 nm was measured. Contrasted to fluorescence, the emission at 509 nm was found to be polarized, following that of the pump beam. However, it should also be noted that supercontinuum generation is also polarized with the pump beam, albeit at different wavelengths as predicted by theory.[31,32]

B. Concentration Dependent Saturation Intensity. The results of Volkmer et al.,[5] Schwille et al.,[9] and our previous work[8] are shown in Figure 4 (open circles). On a log−log plot of these data, there appears to be a nearly cubic (2.7) dependence of the saturation intensity on the concentration of GFP molecules. Extrapolating this trend to fit the 352 μM (2.12×10^{17} cm^{-3}) concentration used in our current experiment shows the value obtained in our fit for the gain follows this dependence. The solid line is the extrapolation of the fit to the lower three data points. To explain the concentration dependence of the saturation intensity, each of the terms contributing to the saturation intensity discussed above were investigated.

The dimerization of GFP was measured by calculating the ratio of the 396 nm (monomer) to 476 nm (dimer) excitation peak as a function of GFP concentration. The results are shown in Figure 5. An excitation spectrum of GFP is shown in the inset of Figure 6, where the peak at 395 nm corresponds to monomer dominant absorption and the peak at 475 nm corresponds to dimer dominant absorption. Note that as the concentration is increased, the ratio of the monomer peak to dimer peak decreases, which suggests the significant formation of

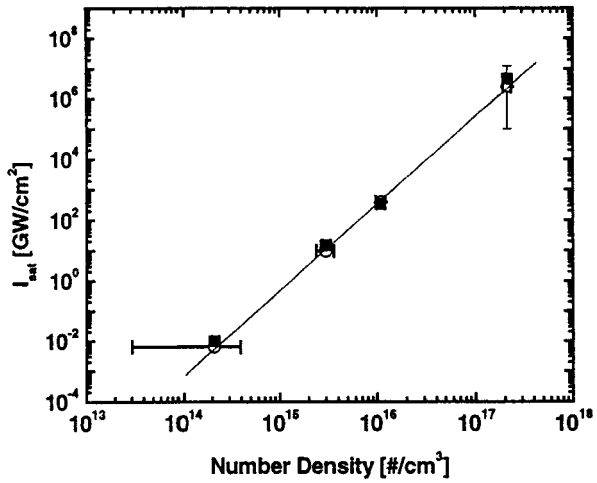

Figure 4. Saturation Intensity as a function of GFP number density. The results of Volkmer et al.,[5] Schwille et al.,[9] our current findings, and our previous work[8] are shown as open circles. The solid line is the extrapolation of the fit to the lower three data points having a slope of 2.7 ± 0.1. The solid squares are the values obtained by taking the theoretical contributions of the concentration on each individual component of the saturation intensity (eq 2).

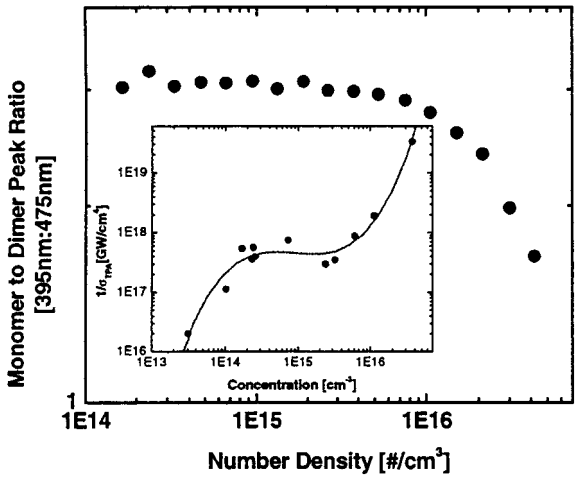

Figure 5. The ratio of the 396 nm (monomer) to 476 nm (dimer) excitation peak of GFP as a function of GFP concentration is given as solid dots. The inset shows the log of the inverse of the TPA cross section as a function of concentration. The solid line is a cubic fit performed to the experimental data in order to determine the functional form between the inverse of the TPA cross section and the GFP concentration.

dimers beginning at approximately 5×10^{15} cm^{-3}. This value corresponds well to that reported for wild-type GFP by Ward et al.[34] This ratio also takes into account the slight red shift in the excitation peaks, evident in the spectra, and consistent with dimer formation.

From these data, the monomer excitation peak normalized to the total concentration was also found and is shown in Figure 6. The solid line is the fit to the data, giving a slope equal to 0.43. One can conclude therefore, that the probability function $\rho(2\omega)$ has a nonzero concentration dependence approaching the power of $^1/_2$.

The effect of the dimer formation on the TPA cross section is shown in the inset of Figure 5. Referring back to eq 2, with the TPA cross section being inversely proportional to the saturation intensity, the inverse of the TPA cross section is plotted here as a function of concentration. As the concentration of GFP is increased, and hence as the number of dimers increases, there is a reduction of the TPA cross section. Note

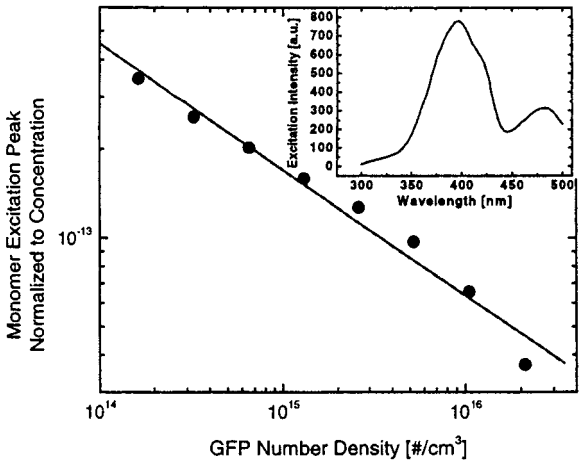

Figure 6. The solid circles are the monomer excitation peak normalized to the total concentration as a function of GFP number density. The solid line is the fit to the data, giving a slope equal to 0.43. The inset is a typical excitation spectrum of GFP as a function of wavelength showing the two peaks at 476 nm (dimer dominated) and 396 nm (monomer dominated).

that the sharp decrease in the cross section corresponds to the significant formation of dimers around 5×10^{15} cm^{-3}. A cubic fit was performed to the data to obtain the functional form between the $\log(1/\sigma_{TPA})$and the concentration of GFP molecules. Also note that, as the TPA cross section shows a clear concentration dependence, one can argue that the multipolar contribution to the fluorescence quenching is not dominant as discussed above and in agreement with De Angelis et al.[35]

Combining these contributions with the theoretical contribution of the homogeneous line width (linear in number density), and no dipole−dipole energy transfer interaction, the overall dependence of the saturation intensity with respect to the concentration is plotted in Figure 4 as solid squares. The dominant contributing term is the TPA cross section. The results yield a reasonable overlap with the data, suggesting a collective explanation for the concentration dependence of the saturation intensity of GFP, dominated by the dimer contribution to the TPA cross section.

V. Conclusions

The first demonstration of ultrafast two-photon lasing in a biological system has been reported. Visible light centered at 509 nm is produced from a micro-cavity of GFP when pumped with an ultrafast IR (790 nm) beam. The lasing threshold was determined to be $4.9\ \mu J \pm 0.8\ \mu J$. Beyond this threshold value, the experimental characteristics of GFP show an increase in output energy (consistent with the saturation model of the two-photon cross section) and a narrowing of the spectral bandwidth. These factors along with a polarization dependence of the output signal collectively suggest lasing as opposed to fluorescence. However, to increase the efficiency of the GFP lasing system, optimization of the experimental conditions is needed.

The apparent cubic dependence of the saturation intensity on the concentration of GFP molecules was also investigated. The theoretical factors that influence the saturation intensity (inhomogeneous line shape, homogeneous line width, TPA cross section, and lifetime of the two-photon state) were explored individually to determine their respective dependence as a function of GFP concentration. A theoretical model based on the individual components of the saturation intensity was fit to the experimental data to give a possible explanation to the cubic

dependence, suggesting a dominant contribution of the TPA cross section from the dimerization of GFP.

References and Notes

(1) Misteli, T.; Spector, D. L. *Nat. Biotechnol.* **1997**, *15*, 961.

(2) Kojima, S.; Hirano, T.; Niwa, H.; Ohashi, M.; Inouye, S.; Tsuji, F. *Tetrahedron Lett.* **1997**, *38*, 2875.

(3) Chattoraj, M.; King, B. A.; Bublitz, G. U.; Boxer, S. G. *Proc. Nat. Acad. Sci. U.S.A.* **1996**, *93*, 8362.

(4) Xu, C.; Zipfel, W.; Shear, J. B.; Williams, R. M.; Webb, W. W. *Nat. Acad. Sci. U.S.A.* **1996**, *93*, 10763.

(5) Volkmer, A.; Subramaniam, V.; Birch, D. J. S.; Jovin, T. M. *Biophys. J.* **2000**, *78*, 1589.

(6) Maruo, S.; Kawata, S. *J. Microelectromechanical Systems* **1998**, *7*, 411.

(7) Kirkpatrick, S. M.; Baur, J. W.; Clark, C. M.; Denny, L. R.; Reinhardt, B. R.; Kannan, R.; Stone, M. O. *Appl. Phys. A* **1999**, *69*, 1.

(8) Kirkpatrick, S. M.; Naik, R. R.; Stone, M. O. *J. Phys. Chem. B* **2001**, *105*, 2867.

(9) Schwille, P.; Haupts, U.; Maiti, S.; Watt, W. *Biophys. J.* **1999**, *77*, 2251.

(10) Silversmith, A. J.; Lenth, W.; Mcfarlane, R. M. *Appl. Phys. Lett.* **1987**, *51*, 1977.

(11) Pollack, S. A.; Chang, D. B.; Birnbaum, M. *Appl. Phys. Lett.* **1989**, *54*, 869.

(12) Nguyen, D. C.; Faulkner, G. E.; Dulick, M. *Appl. Opt.* **1989**, *28*, 3553.

(13) McFarlane, R. A. *Appl. Phys. Lett.* **1989**, *54*, 2301.

(14) Mita, Y.; Wang, Y.; Shionoya, S. *Appl. Phys. Lett.* **1993**, *62*, 802.

(15) Allain, J. Y.; Monerie, M.; Poignant, H. *Electron. Lett.* **1990**, *26*, 261.

(16) Smart, R. G.; Hanna, D. C.; Tropper, A. C.; Davey, S. T.; Carter, S. F.; Szebesta, D. *Electron. Lett.* **1991**, *27*, 1307.

(17) Whitley, T. J.; Millar, C. A.; Wyatt, R.; Brierley, M. C.; Szebesta, D. *Electron. Lett.* **1991**, *27*, 1785.

(18) Grubb, S. G.; Bennett, K. W.; Cannon, R. S.; Hunter, W. F. *Electron. Lett.* **1992**, *28*, 1243.

(19) Patel, C. K. N.; Fleury, R. E.; Slusher, R. E.; Firsch, H. L. *Phys. Rev. Lett.* **1966**, *16*, 971.

(20) Yoshida, T.; Miyazaki, K.; Fujisawa, K. *Jpn. J. Appl. Phys.* **1975**, *14*, 1987.

(21) Gribkovskii, V. P.; Zaporozhchenko, V. A.; Ivanov, V. A.; Kachinskii, A. C.; Parashchuk, V. V.; Yablonskii, G. P. *Sov. J. Quantum Electron.* **1979**, *9*, 1305.

(22) Yang, X. H.; Hays, J. M.; Shan, W.; Song, J. J.; Cantwell, E. *Appl. Phys. Lett.* **1993**, *62*, 1071.

(23) He, G. S.; Brawalker, D.; Zhao, C. F.; Prasad, P. N. *IEEE J. Quantum Electron.* **1996**, *32*, 749.

(24) He, G. S.; Brawalker, D.; Zhao, C. F.; Park, C. K.; Prasad, P. N. *Opt. Lett.* **1995**, *20*, 2393.

(25) He, G. S.; Brawalker, D.; Zhao, C. F.; Park, C. K.; Prasad, P. N. *Appl. Phys. Lett.* **1996**, *68*, 3549.

(26) He, G. S.; Yuan, L.; Cui, Y.; Li, M.; Prasad, P. N. *J. Appl. Phys.* **1997**, *81*, 2529.

(27) He, G. S.; Yuan, L.; Prasad, P. N.; Abbotto, A.; Facchetti, A.; Pagani, G. A. *Opt. Commun.* **1997**, *140*, 49.

(28) He, G. S.; Kim, K. S.; Yuan, L.; Cheng, N.; Prasad, P. N. *Appl. Phys. Lett.* **1997**, *71*, 1619.

(29) He, G. S.; Signorini, R.; Prasad, P. N. *App. Opt.* **1998**, *37*, 5720.

(30) Saleh, B. E.; Teich, M. C. *Fundamentals of Photonics*; Wiley-Interscience: New York, 1991.

(31) Alfano, R. A. *The Supercontinuum Laser Source*; Springer-Verlag: New York, 1989.

(32) Diels, J. C.; Rudolph, W. *Ultrashort Laser Pulse Phenomena*; Academic: San Diego, 1996.

(33) Huang, K. *Statistical Mechanics*; John Wiley & Sons: New York, 1987.

(34) Ward, W. W. *Green Fluorescent Protein: Propoerties, Applications, and Protocols*; Chalfie, M., Kain, S., Eds.; Wiley-Liss: New York, 1998.

(35) DeAngelis, D. A.; Miesenbock, G.; Zemelman, B. V.; Rothman, J. E. *Proc. Natl. Acad. Sci. U.S.A.* **1998**, *95*, 12312.

(36) Henderson, B.; Imbusch, G. F. *Optical Spectroscopy of Inorganic Solids*; Oxford Science: New York, 1989.

(37) Sheik-Bahae, M.; Said, A. A.; Wei, T−H.; Hagan, D. K.; Van Stryland, E. W. *IEEE J. Quantum Electron* **1990**, *QE−26*, 760.

(38) Yariv, A. *Quantum Electronics*; John Wiley & Sons: New York, 1989.

(39) Newport Corporation *Optics and Mechanics Catalog*; Irvine, CA, 1999.